

Field-Emission Resonances at Tip/ α,ω -Mercaptoalkyl Ferrocene/Au Interfaces Studied by STM

Lars Müller-Meskamp, Silvia Karthäuser,* Harold J. W. Zandvliet, Melanie Homberger, Ulrich Simon, and Rainer Waser

The electrical properties of α,ω -mercaptoalkyl ferrocenes with different alkyl chain lengths embedded in a self-assembled host matrix of alkanethiols on Au(111) are studied by scanning tunneling microscopy and spectroscopy. Based on current–distance spectroscopy, as well as on the evaluation of Fowler–Nordheim tunneling current oscillations, the apparent barrier height of ferrocene is determined independently by two methods. The electronic coupling of the ferrocene moiety to the Au(111) substrate is shown to depend on the length of the alkane-spacer chain. In a double tunnel junction model our experimental findings are explained, addressing the role of the different molecular moieties of the mercaptoalkyl ferrocenes.

Keywords:

- charge transfer
- ferrocene
- field-emission resonance
- scanning tunneling microscopy
- self-assembled monolayers

1. Introduction

The ability to access and use electronic properties of individual molecules together with the inherent capability of self-organization promises new possibilities for future nanoelectronic devices. Especially interesting for applications in electronic devices are molecules with reliable redox behavior, which have the potential to be used as switches or storage elements. However, a prerequisite for the realization of such devices is the understanding of the electronic properties of the respective molecules in well-defined structures.

In this work, we focus on one class of stable metal organic compounds, α,ω -mercaptoalkyl ferrocenes (IUPAC name: 11-(mercaptoalkyl), which are known to show reversible redox behavior in solution and can be modified by standard chemical methods.^[1,2] Ferrocene derivatives may act as donors in

donor/acceptor systems similar to those proposed by Aviram and Ratner or, by using the properties of the central iron atom, might be employed as spin valves or as part of a molecular wire.^[3–5]

Mercaptoalkyl ferrocenes that form self-assembled monolayers (SAMs) on Au(111) were studied by electrochemical methods, showing successful chemisorption on gold surfaces, intact redox behavior, and charge transfer kinetics of the chemisorbed species in solution.^[6,7] Besides layers of pure ferrocenes, mixed layers with alkanethiols were also realized, which provide access to the assembly dynamics of SAMs by monitoring the redox behavior during layer formation.^[8,9] The self-assembled ferrocene layers show a tendency to form multilayer structures, as revealed by ellipsometry, and reversible thickness changes upon oxidation/reduction. The latter changes are attributed to a flipping of the ferrocene end-group or a swing of the alkyl chain.^[10–13] A negative differential resistance (NDR) effect for SAMs of α,ω -mercaptoundecanyl ferrocene discovered by scanning tunneling spectroscopy (STS) could later be attributed to the presence of oxygen, causing irreversible chemical changes in the material.^[14–16]

In this study the electrical properties of chemisorbed, standing-up α,ω -mercaptoalkyl ferrocenes are studied by ultra-high-vacuum STS (UHV-STS). To minimize the configurational freedom of the chemisorbed molecules, the matrix isolation approach is chosen. The mercaptoalkyl ferrocene molecules are embedded into SAMs of alkanethiols, which serve as well-defined host matrices with known electrical and

[*] Dr. S. Karthäuser, Dr. L. Müller-Meskamp, Prof. R. Waser
Institute for Solid State Research (IFF) and JARA-FIT
Research Center Juelich GmbH, 52425 Jülich (Germany)
E-mail: s.karthauser@fz-juelich.de
Prof. H. J. W. Zandvliet
Mesa + Institute for Nanotechnology, University of Twente
7500 AE Enschede (The Netherlands)
Dr. M. Homberger, Prof. U. Simon
Institute of Inorganic Chemistry (IAC) and JARA-FIT,
RWTH Aachen University
Landoltweg 1, 52074 Aachen (Germany)

structural properties. Using current–distance (I – s) and current–voltage (I – U) spectroscopy, we demonstrate that the apparent tunneling barrier height of ferrocenes can be determined both from I – s measurements, as well as from oscillations in the tunneling current that occur at voltages exceeding the barrier height (Gundlach oscillations or field emission resonance (FER)).

2. Current–Distance Spectroscopy

Short-chain mercaptoalkyl ferrocenes (Fc-(CH₂)_{*n*}-SH, abbreviated FcC*n*), such as FcC3, inserted into an octanethiol matrix form a monolayer structure as shown in Figure 1. The self-assembled alkanethiol monolayer remains visible in the mixed monolayer with its characteristic features such as domain boundaries, monolayer-deep etch pits, and the hexagonal packing of the molecules with the characteristic $c(4 \times 2)$ superlattice referring to a well-ordered monolayer.^[17] After insertion the ferrocene derivatives form surface ribbons along the domain boundaries, visible as blurry features decorating the ordered alkanethiol domains (Figure 1). Annealing of the mixed monolayers in vacuum leads to a partial order of the ferrocene ribbons and even domains or islands with regular ferrocene structures can be identified.^[18,19] From structural investigations the occupied area per mercaptoalkyl ferrocene molecule was determined to be 0.50 nm² for FcC3 and 0.61 nm² for FcC5 and FcC11, which is more than twice the area needed for an alkanethiol molecule (0.216 nm²).^[17]

The electrical transport through FcC*n* molecules embedded in a C*n* SAM matrix was characterized first by I – s spectroscopy, a well-accepted method to characterize the chemical specificity of the sample surface and the local electronic charge. These measurements were performed on regular structures of α,ω -mercaptoalkyl ferrocenes similar to the structures shown in Figure 1, and for comparison on ordered domains of dodecanethiol as well. The spectra

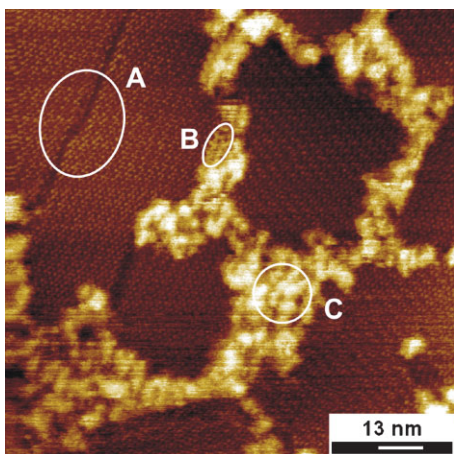


Figure 1. Typical topography of FcC3 embedded into a C8 SAM. The ordering of the host monolayer is visible, showing the alkanethiol $c(4 \times 2)$ surface texture and domain boundaries (A). Mercaptoalkyl ferrocenes are inserted at C8 domain boundaries (C) and beginning formation of ferrocene domains (B) is visible.

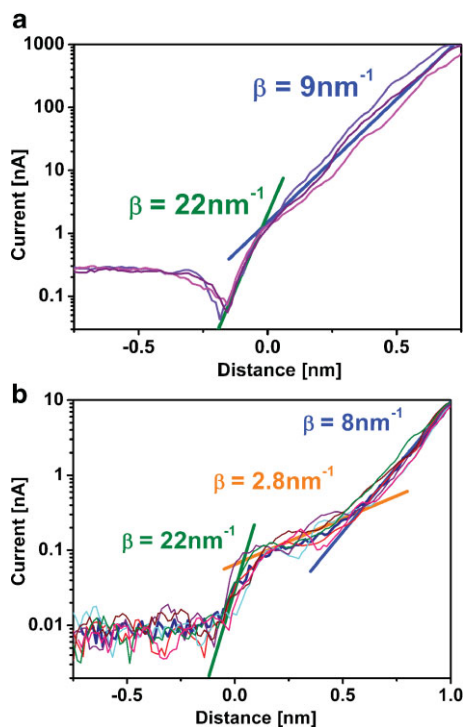


Figure 2. I – s spectroscopy on C12 (a) and mercaptoundecyl ferrocene (b). The slopes in the semilogarithmic I – s plot reflect the decay constants.

recorded on C12 and on extended patches of FcC11 inserted into C12 are shown in Figure 2.

A 1D tunneling model to describe the charge transport from the scanning tunneling microscopy (STM) tip through the vacuum and the molecular layer to the gold surface was considered. This model is applicable for large barrier heights and small barrier widths. As the tip approaches towards the surface the tunneling current (I_t) depends exponentially on the distance, which in the Wentzel–Kramers–Brillouin (WKB) approximation for a 1D square potential barrier leads to

$$I_t \propto U \exp\left(-\frac{4\pi\sqrt{2m^*}}{h} \sqrt{\phi_B z}\right) \quad (1)$$

and

$$\beta = \frac{4\pi\sqrt{2m^*}}{h} \sqrt{\phi_B} \quad (2)$$

for low currents, $eU \ll \phi_B$, where e = electron charge, U = bias voltage, m^* is the effective electron mass, ϕ_B is the apparent tunneling barrier height, z is the tip–surface distance, h is Planck's constant, and β is the tunneling decay constant.^[20] Therefore, the slope of a semilogarithmic plot of the recorded tunneling current versus tip displacement is proportional to the tunneling decay constant of the respective material. This approach can be used to extract the apparent tunneling barrier height.

Figure 2, a characteristic graph of I - s measurements for alkanethiols, starts with a noisy low-current branch for large tip-sample distances, when the current is in the range of the noise level of the preamplifier. Upon approaching the surface a steep increase in current is visible. The slope in this branch is governed by a vacuum decay constant of $\beta_{\text{vac}} = 22 \text{ nm}^{-1}$. When the tip starts to penetrate the dodecanethiol monolayer a sharp bend in the I - s curve appears, defining the contact point, and the slope is reduced to a value of 9 nm^{-1} , attributed to the lower apparent barrier height of the alkane backbone, $\phi_{\text{B}}(\text{CH})$, as compared to vacuum. The I - s measurements obtained for FcC11 (Figure 2) show an additional feature. The spectra recorded on FcC11 exhibit a sharp transition after the contact point, followed by an additional regime with a strongly reduced slope of $\approx 2.8 \text{ nm}^{-1}$, and after a distance of $\approx 0.4 \text{ nm}$ a second increase in the current slope to a value of $\approx 8 \text{ nm}^{-1}$ is observed. The plateau in the current slope corresponding to a locally reduced decay parameter is attributed to the ferrocene end-groups on top of the monolayer. This is reasonable due to spatial considerations for the FcC11 SAM, taking into account a distance of 0.39 nm between the cyclopentadienyl (Cp) rings of a ferrocene moiety (Figure 2). The decay constant of 8 nm^{-1} for the further movement into the monolayer is comparable to the value expected for the alkanethiols from the previous measurements. One reason for the slight deviation of the decay constant compared to the pure alkanethiols is probably the different packing density of the mercaptoalkyl ferrocenes compared to the alkanethiols, for example, 0.61 nm^2 per ferrocene derivative compared to 0.21 nm^2 per alkanethiol. Another reason might be the electronic influence of the ferrocene moiety attached to the alkane chain. The I - s curve of the ferrocene derivative FcC3 (not shown), also exhibits a regime with a strongly reduced slope, $\beta_{\text{Fc}} \approx 2.8 \text{ nm}^{-1}$ very similar to FcC11, but the regime of again increased slope, $\beta_{\text{CH}} \approx 8 \text{ nm}^{-1}$, is not visible. From spatial considerations, this effect can be explained by the very short alkane chain that is entangled with the bulky ferrocene moieties and not long enough to establish a tunneling regime that is unaffected by the substrate or the ferrocene layer.

I - s spectroscopy on mercaptoalkyl ferrocenes in our measurement setup clearly proves that the decay constant is not constant over the entire length of the system, but depends strongly on the nature of the respective material. Three different parts of the I - s curve with different decay constants can be identified: the tunneling gap between the STM tip and the molecule (β_{vac}), the ferrocene moiety (β_{Fc}), and the alkane chain (β_{CH}).

$$I_t \propto \exp(-\beta_{\text{vac}}z_{\text{vac}} - \beta_{\text{Fc}}z_{\text{Fc}} - \beta_{\text{CH}}z_{\text{CH}}) \quad (3)$$

This is very similar to the case of biphenylethanethiols.^[21] Figure 3 shows a schematic illustration of the mercaptoalkyl ferrocene monolayer including the different decay constants that are involved in the tunneling process.

The experimentally obtained tunneling decay constant for the vacuum, $\beta_{\text{vac}} = 22 \text{ nm}^{-1}$, is in good agreement with values reported in literature.^[22,23] Using Equation 1, $\beta_{\text{vac}} \approx 22 \text{ nm}^{-1}$ and $m^* = m_e$ for metals (m_e), a value for the apparent barrier

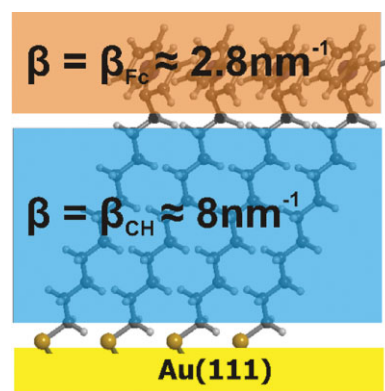


Figure 3. Schematic illustration of FcC11 in a SAM with an assignment of the decay constants to the ferrocene moiety and the alkane chain.

height of 4.6 eV results, which is in the typical range for metallic surfaces.^[24,25] The experimental values of the tunneling decay constant of the alkane backbone are also in good agreement with values reported in literature, that is, 8.8 , 7 , and 11 nm^{-1} for alkanethiols.^[26–28] Recent reviews give a good overall view on the variation of tunneling decay constants depending on the exact experimental configuration.^[20,29] Using Equation 1 and assuming $m^* = 0.42 m_e$, obtained using the Simmons Model to fit alkanethiol tunneling parameters, the values of $\beta_{\text{CH}} = 9$ and 8 nm^{-1} correspond to $\phi_{\text{B}}(\text{CH})$ of 1.83 eV and 1.45 eV , respectively, which are also in good agreement with Reed.^[29] It should be pointed out that Equation 1 is only valid for voltages reasonably smaller than the apparent barrier height, in the case of alkanethiols up to approximately 1 V .

Applying again the same procedure as mentioned above to deduce the apparent tunneling barrier height for the ferrocene moiety, $\phi_{\text{B}}(\text{Fc})$, from $\beta_{\text{Fc}} = 2.8 \text{ nm}^{-1}$, results in values smaller than 0.2 eV depending on the exact value of m^* . However, this small value of $\phi_{\text{B}}(\text{Fc})$ implies that Equation 1 is no longer applicable here, since $eU > \phi_{\text{B}}(\text{Fc})$. In the case of mercaptoalkyl ferrocenes a bias voltage of $\pm 1 \text{ V}$ is high enough to be remarkably larger than the apparent barrier height. This causes the tunneling barrier shape to change from a trapezoidal barrier, characteristic for direct tunneling, to a triangular barrier whose properties are changed with increasing voltage. Tunneling through a triangular barrier, where the electrons tunnel into the conduction band of a dielectric, is called Fowler–Nordheim tunneling or field emission.^[29] In this case we can use the following expression for the tunneling current

$$I_t \propto U^2 \exp\left(-\frac{8\pi\sqrt{2m^*}}{3ehU}\phi_{\text{B}}^{3/2}z\right) \quad (4)$$

and

$$\beta_{\text{FN}} = \frac{8\pi\sqrt{2m^*}}{3 \cdot e \cdot h \cdot U} \cdot \phi_{\text{B}}^{3/2} = \frac{6.826}{U} \cdot \phi_{\text{B}}^{3/2} \quad (5)$$

Assuming $m^* = m_e$, and using the experimentally determined $\beta_{\text{Fc}} = 2.8 \text{ nm}^{-1}$ and Equation 4 to determine the

apparent tunneling barrier height leads to a value of $\phi_B(\text{Fc}) = 0.62 \text{ eV}$ for the ferrocene moiety. This is a rather low value as compared to other molecules.

3. Voltage-Dependent Imaging

Using the matrix isolation approach, mercaptoalkyl ferrocenes embedded into an alkanethiol matrix have the appealing advantage that the highly ordered alkanethiol domains may serve as geometrical and electrical reference. The latter should be kept in mind in interpreting and discussing the next images. In the experiments shown in Figure 4, the step height between ordered surface domains of FcC3 and the surrounding C8 monolayer is measured in constant-current mode for bias voltages ranging from -0.8 to -1.8 V using UHV-STM. It is obvious from the selected images that the apparent height of the ferrocene derivatives depends strongly on the bias voltage. This behavior has not been observed so far for other molecules inserted in an alkanethiol matrix. For lower bias voltages only slightly elevated features are visible, whereas for higher negative bias bright, well-defined features appear. The resulting apparent height differences, plotted into a diagram versus bias voltage (Figure 5), show a strong increase for bias voltages exceeding -1.5 V .

A comparable behavior of FcC11 islands embedded into a decanethiol SAM was observed using STM under an electrochemical environment.^[30] The apparent heights of the FcC11 islands with respect to the surrounding C10 matrix were enhanced with increased sample bias. Yokota et al. stated that the apparent heights are not correlated with the island size, irrespective of the oxidation state of the ferrocene moiety, which rules out an intermolecular conduction path as major conduction mechanism. Furthermore, it was demonstrated that the positive charge is not a prerequisite to amplify the STM current through FcC11 islands.^[30] This is in accordance with our findings, because a charging of the monolayer in vacuum is rather unlikely. Due to the lack of counter ions in vacuum only a very limited amount of charging is possible so that in our case the FcC3 molecules are assumed to be uncharged. This does not exclude the interim appearance of charged molecular states with short lifetimes during the tunneling process.

The monitored changes of the apparent height (Figure 5), as obtained from STM measurements, could originate from geometric or electronic changes in the mixed monolayer. But due to the monotonous increase and the absolute value of the

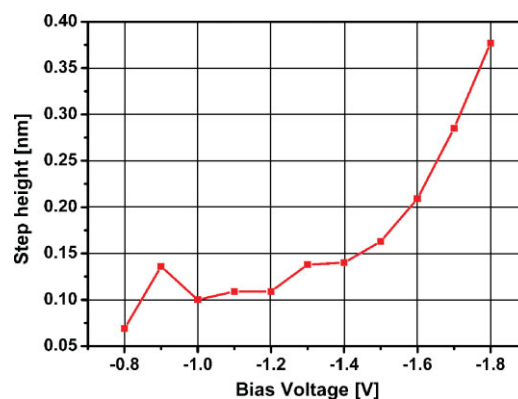


Figure 5. The resulting height difference between FcC3 and C8, measured at location B as outlined in Figure 1, is plotted against the bias voltage and shows a strong exponential dependence.

increase ($\approx 0.35 \text{ nm}$) a redox-induced geometric thickness change can be excluded. Yao et al. observed a monolayer thickness change of FcC11 of about 0.09 nm resulting from the oxidation of ferrocene to ferrocenium in water.^[13] A possible explanation for this thickness change is a rotation or flipping of the ferrocene moiety around the bond between the ferrocene moiety and the alkyl chain or, more likely, a swinging of the alkyl chain farther away from the electrode ($\approx 2.7^\circ$). These effects are not monotonous and cannot account in size for our findings. Therefore we conclude that the apparent step height changes of FcC3 with respect to C8 as a function of applied bias voltage, U_b , are mainly electronic in origin.

The step height changes are causally related to the electronic properties of the molecules under study, that is, FcC3 and C8, and the matrix isolation approach. The molecules used as electronic reference are octanethiols, whose conduction mechanism is widely accepted to fall into the direct tunneling regime. This means that the tip-surface distance on C8 domains is related to the current as $z_{\text{CH}} \sim \ln I = \text{constant}$. In contrast, the conduction mechanism of ferrocene derivatives for $U_b > 0.6 \text{ V}$ falls into the Fowler-Nordheim regime as shown in the previous section. Therefore, the tip-surface distance on FcC3 domains shows the following dependence on current and sample bias: $z_{\text{Fc}} \sim U \ln(I/U^2)$, which is obviously strongly dependent on the bias voltage and will increase with increasing voltage. Taking the difference ($z_{\text{CH}} - z_{\text{Fc}}$), which is exactly the step height, results in a curve like the one in Figure 5. This behavior confirms Fowler-Nordheim tunneling as the conduction mechanism in ferrocene derivatives.

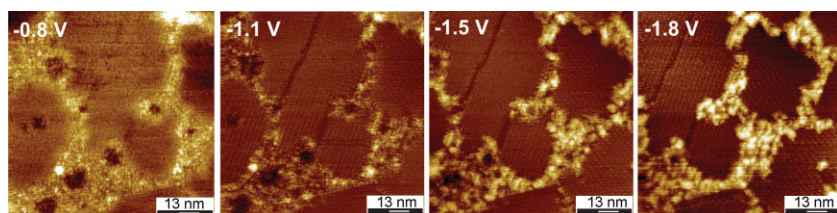


Figure 4. Voltage-dependent imaging of the structure shown in Figure 1. The mercaptoalkyl ferrocenes appear brighter at higher bias voltages.

4. Current-Voltage Spectroscopy

$I-U$ spectroscopy of mercaptoalkyl ferrocenes with different chain lengths (FcCn with $n = 3, 5,$ and 11) inserted into the corresponding alkanethiol host matrices has been performed. In Figure 6 the obtained $I-U$ curves are compared. For

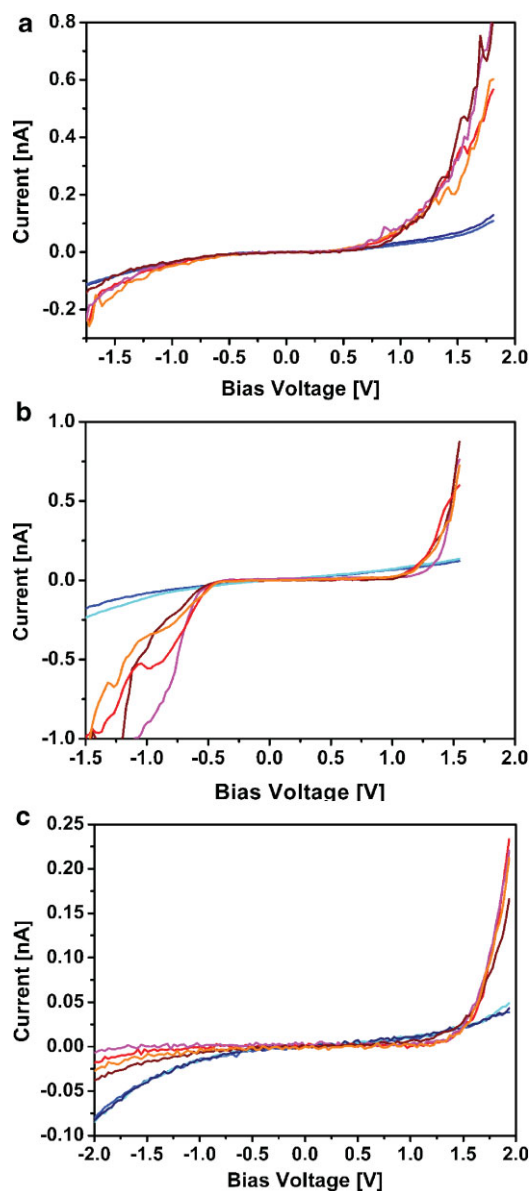


Figure 6. I - U spectroscopy on mercaptoalkyl ferrocenes with different chain lengths embedded into the respective alkanethiol monolayer. a) FcC3, b) FcC5, and c) FcC11. The diagrams compare the I - U curves of the ferrocenes (red) with the host alkanethiol matrices (blue).

all three diagrams a pronounced increase in current of the ferrocene derivatives is observed at higher voltages. It is remarkable that the conduction threshold is found at higher voltages for mercaptoalkyl ferrocenes with longer alkane chains. These I - U curves from UHV-STM do not show an NDR effect (in accordance with Reference [16]) or a sudden change, which could be attributed to a redox behavior. But most interestingly, a characteristic increase in current is observed when the applied bias voltage exceeds $\phi_B(\text{Fc})$ due to the onset of Fowler-Nordheim tunneling. The change in transport mechanism from direct tunneling to the field emission regime can be determined by plotting $\ln(I/U^2)$ versus $1/U$ from the change in slope. Using the relationship given in Reference [31] we obtained data curves qualitatively similar to literature data and an inflection point, U_{trans} , of

0.3 V, which characterizes the transition from direct tunneling to Fowler-Nordheim tunneling. However, the barrier height determined by this method usually is significantly lower than estimated, for example, by ultraviolet photoelectron spectroscopy (UPS) and thus gives only a lower limit for the potential barrier.^[31]

How the onset of Fowler-Nordheim tunneling can be influenced by the alkane-spacer-chain length is demonstrated in the schematic energy diagram shown in Figure 7. The ferrocene moiety of FcCn is assumed to form a quantum well separated from two electrical contacts, the tip and the gold substrate, by two tunnel barriers. The tip/ferrocene barrier is simply the vacuum gap, whereas the ferrocene/gold barrier is due to the alkane-spacer chain, which also defines this barrier width. Hence for a fixed sample bias the voltage drop over the vacuum gap is relatively smaller for molecules with longer alkane-spacer chains, if the same bias voltage is applied (Figure 7). Therefore, higher bias voltages have to be used in order to overcome the conductance threshold caused by longer alkane-spacer chains in mercaptoalkyl ferrocenes.

Having a closer look at the I - U curves, especially in the case of FcC3 (Figure 6), a distinct “noise” is measured for high bias voltages in the regime where the current increases significantly. For this regime of Fowler-Nordheim tunneling through a triangular barrier with $U_b \gg \phi_B(\text{Fc})$, Gundlach has calculated the tunneling current as a function of U_b .^[32] He

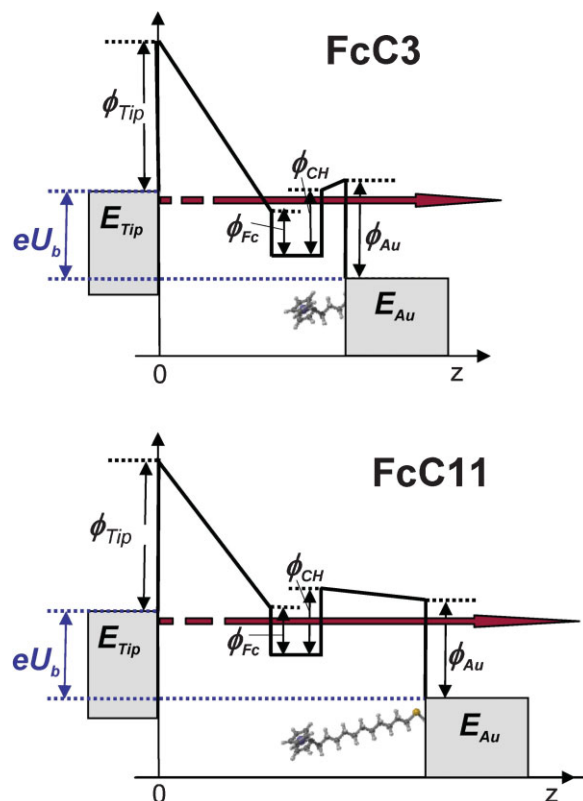


Figure 7. Schematic energy diagram for Fowler-Nordheim tunneling from the tip to the ferrocene moiety and direct tunneling from the ferrocene moiety to the Au(111)-substrate for mercaptoalkyl ferrocenes with $n = 3$ and 11, respectively. E_{Tip} and E_{Au} are the Fermi energies of the tip and the Au(111)-substrate.

found that I_t exhibited additional oscillations resulting from reflected electrons between both barrier boundaries. Thus, for well-defined voltages, electron standing waves in the vacuum gap between emitter (e.g., tip) and collector (e.g., ferrocene moiety) can develop. These electron standing waves lead to an oscillating dependence of the tunneling probability and thus tunnel current as a function of U_b . Thus, the conductance, dt/dU_b , versus U_b curve shows maxima at well-defined voltages U_n with $n = 1, 2, 3, \dots$ (Figure 8). According to van Kempen, who considered a simplified model of a 1D tunnel junction, the following equation can be derived^[33]

$$eU_n = \phi_B + \left(\frac{3\pi}{a}\right)^{2/3} F^{2/3} n^{2/3} \quad (6)$$

with

$$F = \frac{eU_o}{z} \quad (7)$$

and

$$a = \frac{4\pi\sqrt{2m^*}}{h} = 10.25 \frac{1}{\text{nm}\sqrt{\text{eV}}} \quad (8)$$

U_0 denotes the bias voltage of the set-point. Plotting the position of the maxima of the differential conductance versus the order of the resonance to the two-thirds power, $n^{2/3}$ (Figure 9), results in a curve with an intercept at $\phi_B(\text{Fc})$. The obtained value of 0.60 eV is in excellent agreement with the value of 0.62 eV obtained by I - s spectroscopy. Therefore, we have extracted the apparent tunneling barrier height of ferrocene in vacuum by two independent methods. The extremely low barrier height of ferrocene, which is even smaller than the apparent tunneling barrier height for oligophenylenes, explains all the experimentally received UHV-STM and STS data in a satisfactory way.

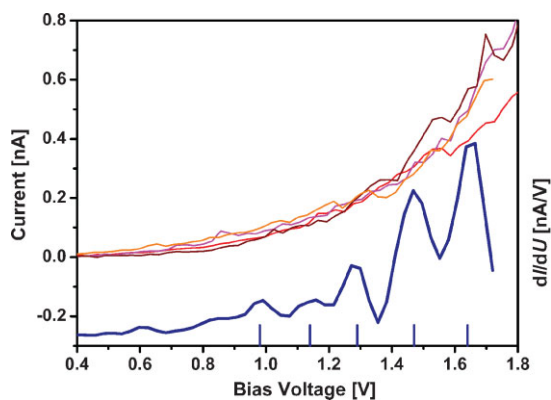


Figure 8. I - U curves of FcC3 (red) and differential conductance (blue) showing Fowler-Nordheim tunneling with superimposed Gundlach oscillations.

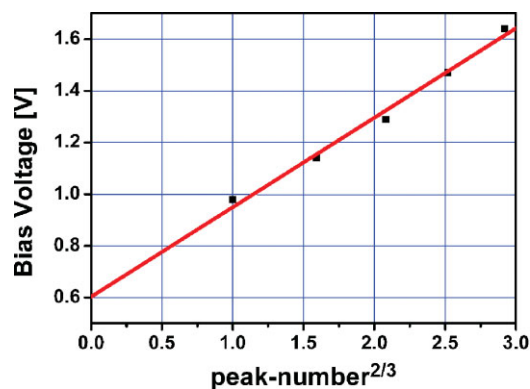


Figure 9. Plot of the maxima of the differential conductance versus the order of the resonance to the power two-thirds.

5. Conclusion

Two UHV-STs methods, I - s spectroscopy and I - U spectroscopy were applied successfully on ordered domains of mercaptoalkyl ferrocenes embedded into alkanethiols. The results are in excellent agreement and reveal that the main conduction mechanism of ferrocene is Fowler-Nordheim tunneling. Furthermore, Gundlach oscillations are clearly observed in the I - U spectra. The apparent tunneling barrier height of ferrocene is estimated to be 0.60 ± 0.05 eV. The onset of the Fowler-Nordheim tunneling can be additionally modulated by the attached alkane-spacer chains. Thus, ferrocene moieties are attractive candidates to tailor electron transport properties.

6. Experimental Section

Octanethiol (C8) and dodecanethiol (C12) were purchased from Aldrich and used without further purification. The α,ω -mercaptoalkyl ferrocenes (FcC n with $n = 3, 5, 11$) were synthesized and purified according to previously published procedures.^[6,34] All compounds were dissolved in ethanol as millimolar solutions.

As substrates, thin (111)-oriented gold films on mica were prepared as described earlier.^[35] For the formation of mixed monolayers freshly prepared substrates were exposed first to an alkanethiol solution for 24 h and then transferred to a mixed solution of alkanethiols and ferrocenes for 10–120 min or to a pure solution of ferrocenes for 10–30 min. The samples were heated in solution or in vacuum to improve the layer quality and desorb physisorbed molecules from the surface. After deposition, the monolayers were dipped into hot ethanol, thoroughly rinsed, and immediately transferred to vacuum.

The samples were characterized with a JEOL 4500 UHV-STM using homemade electrochemically etched tungsten tips in UHV at a base pressure of 5×10^{-10} mbar. Topographical images were recorded in constant-current mode at bias voltages in the range of ± 1 V to ± 2 V and tunneling currents between 30–100 pA. The structural details of pure and mixed monolayers of mercaptoalkyl ferrocenes as well as the matrix isolation in alkanethiol mono-

layers, as used in this work, are described in earlier publications.^[18,19,36]

I-*s* spectroscopy data were collected on several islands of mercaptoalkyl ferrocenes embedded into an alkanethiol matrix. The tip was placed at various positions on the islands, usually at a U_b of 0.8–1.6 V and set-point currents of 20–50 pA to define the distance to the substrate. Then the feedback was deactivated and the tip retracted and moved towards the surface by 2 nm, while the current signal was recorded. The *I*-*U* curves were collected using the current imaging tunneling spectroscopy (CITS) mode. During a CITS scan a topography image is acquired and at every image point a *I*-*U* curve (–2 V to +2 V) is measured.

Acknowledgements

The authors thank Christina Lennartz, Peter Kowalzik, Hans Haselier, Holger John, Birgit Hahn, and Jutta Kiesgen for their support and the Institute for Functional Materials for Information Technology (IFMIT) for funding.

- [1] R. R. Gagne, C. A. Koval, G. C. Lisensky, *Inorg. Chem.* **1980**, *19*, 2854.
- [2] M. Rosenblum, J. Santer, W. G. Howells, *J. Am. Chem. Soc.* **1963**, *85*, 1450.
- [3] A. Aviram, M. A. Ratner, *Chem. Phys. Lett.* **1974**, *29*, 277.
- [4] R. Liu, S.-H. He, H. U. Barangerand, W. Yang, *Nano Lett.* **2005**, *5*, 1959.
- [5] S. A. Getty, C. Engtrakul, L. Wang, R. Liu, S.-H. Ke, H. Baranger, W. Yang, M. Fuhrer, L. Sita, *Phys. Rev. B: Condens. Matter* **2005**, *71*, 241401.
- [6] K. Uosaki, Y. Sato, H. Kita, *Langmuir* **1991**, *7*, 1510.
- [7] J. F. Smalley, S. W. Feldberg, C. E. Chidsey, M. R. Linford, M. D. Newton, Y.-P. Liu, *J. Phys. Chem.* **1995**, *99*, 13141.
- [8] C. E. Chidsey, C. R. Bertozzi, T. M. Putvinski, A. M. Muijsce, *J. Am. Chem. Soc.* **1990**, *112*, 4301.
- [9] T. Auletta, F. C. van Veggel, D. N. Reinhoudt, *Langmuir* **2002**, *18*, 1288.
- [10] A. S. Viana, L. M. Abrantes, G. Jin, S. Floate, R. H. Nichols, M. Kalaji, *Phys. Chem. Chem. Phys.* **2001**, *3*, 3411.
- [11] T. Ohtsuka, Y. Sato, K. Uosaki, *Langmuir* **1994**, *10*, 3658.
- [12] A. S. Viana, A. Jones, L. Abrantes, M. Kalaji, *J. Electroanal. Chem.* **2001**, *500*, 290.
- [13] X. Yao, J. Wang, F. Zhou, J. Wang, N. Tao, *J. Phys. Chem. B* **2004**, *108*, 7206.
- [14] C. B. Gorman, R. L. Carroll, R. R. Fuieler, *Langmuir* **2001**, *17*, 6923.
- [15] A. V. Tivanski, G. C. Walker, *J. Am. Chem. Soc.* **2005**, *127*, 7647.
- [16] J. He, S. M. Lindsay, *J. Am. Chem. Soc.* **2005**, *127*(1), 1932.
- [17] B. Lüssem, L. Müller-Meskamp, S. Karthäuser, R. Waser, *Langmuir* **2005**, *21*, 5256.
- [18] L. Müller-Meskamp, B. Lüssem, S. Karthäuser, S. Prikhodovski, M. Homberger, U. Simon, R. Waser, *Phys. Status Solidi A* **2006**, *203*, 1448.
- [19] L. Müller-Meskamp, B. Lüssem, S. Karthäuser, M. Homberger, U. Simon, R. Waser, *J. Phys: Conf. Ser.* **2007**, *61*, 852.
- [20] E. A. Weiss, J. K. Kriebel, M.-A. Rampi, G. M. Whitesides, *Philos. Trans. R. Soc. London A* **2007**, *365*, 1509.
- [21] B. Lüssem, L. Müller-Meskamp, S. Karthäuser, M. Homberger, U. Simon, R. Waser, *Langmuir* **2006**, *22*, 3021.
- [22] Y. Yasutake, Z. Shi, T. Okazaki, H. Shinohara, Y. Majama, *Nano Lett.* **2005**, *5*, 1057.
- [23] R. L. McCreery, *Chem. Mater.* **2004**, *16*, 4477.
- [24] L. Olesen, M. Brandbyge, M. R. Sorensen, K. W. Jacobsen, E. Laegsgaard, I. Stensgaard, F. Besenbacher, *Phys. Rev. Lett.* **1996**, *76*, 1485.
- [25] L. Limot, J. Kröger, R. Berndt, A. Garcia-Lekue, W. A. Hofer, *Phys. Rev. Lett.* **2005**, *94*, 126102.
- [26] V. B. Engelkes, J. M. Beebe, C. D. Frisbie, *J. Am. Chem. Soc.* **2004**, *126*, 14287.
- [27] E. Wierzbinski, K. Slowinski, *Langmuir* **2006**, *22*, 5205.
- [28] Y. Yasutake, Y. Azuma, K. Nagano, Y. Majima, *Mater. Res. Soc. Symp. Proc.* **2004**, *782*, 17.
- [29] W. Wang, T. Lee, M. A. Reed, in *Nano and Molecular Electronics Handbook*, (Ed: S. E. Lyshevski), CRC Press, Boca Raton, FL **2007**, Ch. 1, pp. 12–27.
- [30] Y. Yokota, K. Fukui, T. Enoki, M. Hara, *J. Phys. Chem. C* **2007**, *111*, 7561.
- [31] J. M. Beebe, B. Kim, J. W. Gadzuk, C. D. Frisbie, J. G. Kushmerick, *Phys. Rev. Lett.* **2006**, *97*, 026801.
- [32] K. H. Gundlach, *Solid-State Electron.* **1966**, *9*, 949.
- [33] O. Y. Kolesnychenko, Y. A. Kolesnichenko, O. I. Shklyarevskii, H. van Kempen, *Physica B* **2000**, *291*, 246.
- [34] C. B. Gorman, R. L. Miller, K.-Y. Chen, A. R. Bishop, R. T. Haasch, R. G. Nuzzo, *Langmuir* **1998**, *14*, 3312.
- [35] B. Lüssem, S. Karthäuser, H. Haselier, R. Waser, *Appl. Surf. Sci.* **2005**, *249*, 197.
- [36] L. Müller-Meskamp, S. Karthäuser, R. Waser, M. Homberger, U. Simon, *Langmuir* **2008**, *24*, 4577.

Received: June 6, 2008

Revised: September 23, 2008